GEOPHYSICAL RESEARCH LETTERS, VOL. 35, L18614, doi:10.1029/2008GL035206, 2008

Low-frequency interaction between horizontal and overturning gyres in the ocean

M. A. Spall[1]

Received 1 July 2008; revised 23 August 2008; accepted 3 September 2008; published 30 September 2008.

[1] Low-frequency variability of the horizontal circulation in an idealized, eddy-permitting, numerical model drives the dominant mode of low-frequency variability in the meridional overturning circulation. This coupling takes place through the influence of lateral advection in the cyclonic high-latitude boundary current on the mixed layer depth along the boundary. The mean and low-frequency variability of the meridional overturning circulation are well predicted by a diagnostic estimate that assumes the downwelling is controlled by the thermal wind shear within the mixed layer along the boundary, which is in turn determined by a simple balance between lateral advection and surface cooling. The more general result is the demonstration that the mean and low frequency variability of the meridional overturning streamfunction are controlled by the baroclinic pressure gradient within the mixed layer along the boundary, which may be influenced by numerous factors such as low-frequency variability in lateral advection, wind stress, surface buoyancy fluxes, or ice melt and freshwater runoff. **Citation:** Spall, M. A. (2008), Low-frequency interaction between horizontal and overturning gyres in the ocean, *Geophys. Res. Lett.*, *35*, L18614, doi:10.1029/2008GL035206.

1. Introduction

[2] Natural low-frequency variability of the oceanic circulation, in both the overturning and horizontal gyres, has been an area of much study, particularly as it relates to climate variability. Low-frequency variability has been observed in idealized ocean-only models that bears some similarities to the low-frequency variability found in observations and coupled models. Although sometimes present with wind-forcing and with combined heat and fresh water forcing, these decadal modes of variability appear to be predominately due to the thermal forcing at the surface [*Huck et al.*, 2001]. Low-frequency variability also arises naturally in wind-driven models of the ocean circulation. Viscous, low resolution models give unique, steady circulations, however, as the resolution is increased and the viscosity is decreased, multiple steady stable and unstable solutions emerge [*Dijkstra and Katsman*, 1997]. A second type of natural internal variability that arises in wind-forced circulations relates to instability of the meridional flow. Although much weaker than the strong, nearly zonal, separated boundary currents, the meridional flow is susceptible to instability because the stabilizing influence of planetary beta is not felt for zonal flows [*Spall*, 1994; I. Kamenkovich et al., On the structure and dynamics of the zonal jets in the North Atlantic, submitted to *Journal of Physical Oceanography*, 2008]. The resulting perturbations are preferentially zonal, and may give rise to slowly propagating barotropic zonal jets that are similar to what has been observed throughout the world's oceans [*Maximenko et al.*, 2005].

[3] Most idealized studies of buoyancy-forced variability have been carried out at relatively low horizonal resolution (greater than the internal deformation radius). This is due to the long time scale associated with the thermal circulation and the large computational expense required to resolve the internal deformation radius. Most studies of the natural variability of the wind-driven gyres have used quasigeostrophic or adiabatic shallow water dynamics, in part because of the long-time integrations associated with vertical diffusion of heat and the high resolution required to represent the internal modes of variability. The present study uses an idealized primitive equation model at high resolution subject to both wind- and buoyancy-forcing. A dominant mode of variability arises that has its sources in the wind-driven gyres yet imprints its variability onto the deep thermally-forced overturning circulation. The details of the oscillation are dependent on several model parameters, but the basic mechanism of interaction between the horizontal and overturning gyres is not specific to this mode of variability and can be expected to be active in a wide range of situations, including externally forced variability.

2. Internal Variability in an Idealized Model

[4] The hydrostatic version of the MITgcm [*Marshall et al.*, 1997] is configured in a square, flat domain of dimension $L = 3.2 \times 10^6$ m and depth 3000 m with 20 km horizontal resolution and 15 levels in the vertical (grid spacing increasing from 25 m near the surface to 400 m below 1400 m). The Coriolis parameter varies linearly with latitude from 0.68×10^{-4} s^{-1} at the southern boundary to 1.32×10^{-4} s^{-1} at the northern boundary (variation with latitude is 2×10^{-11} m^{-1} s^{-1}).

[5] The model is forced at the surface with a symmetric zonal wind stress pattern defined as $\tau^x = \tau_0 \cos(2\pi(y - y_0)/L)$, where $y_0 = 1.6 \times 10^6$ m is the mid-latitude of the basin and $\tau_0 = 0.15$ N m^{-2}, giving a wind-driven horizontal transport of 46×10^6 m^3 s^{-1} in both gyres.

[6] The model is also forced at the surface by a relaxation of temperature at the uppermost model level towards a specified "atmospheric" temperature, which is a linear function of latitude, $T_a = T_{max} - (T_{max} - T_{min})y/L$ where $T_{max} = 20$°C and $T_{min} = 5$°C, with a relaxation time of 100 days. For an upper layer thickness of 25 m, this gives a

[1]Physical Oceanography Department, Woods Hole Oceanographic Institution, Woods Hole, Massachusetts, USA.

0094-8276/08/2008GL035206$05.00

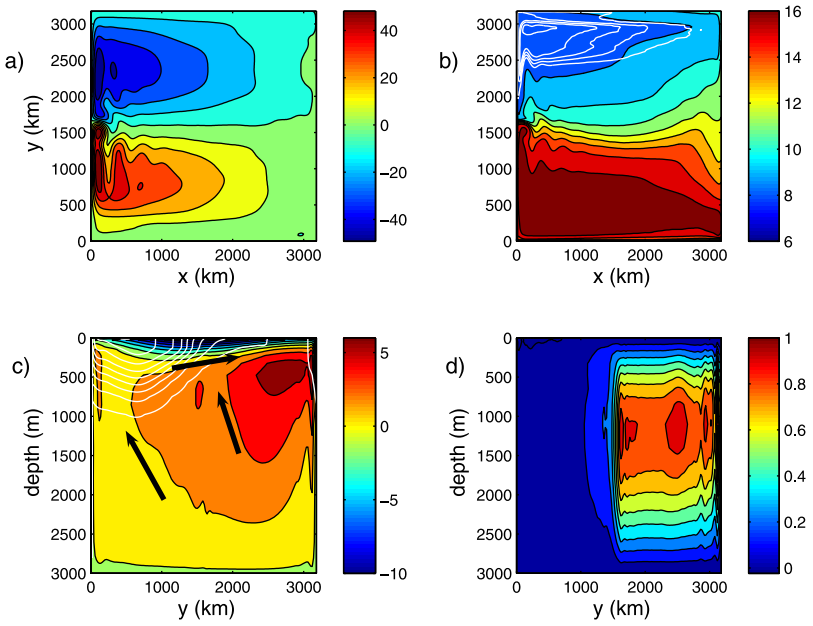

Figure 1. Mean quantities from the final 200 years of integration: (a) horizontal transport streamfunction (10^6 m^3 s^{-1}), (b) temperature at 12.5 m depth (colors) and mixed layer depth (white contours, 500 m contour interval), (c) meridional overturning streamfunction (10^6 m^3 s^{-1}) and isotherms at the mid-longitude of the basin (white contours, 2°C contour interval), and (d) leading empirical orthogonal function of the meridional overturning streamfunction (explains 73% of the variance).

heat flux sensitivity of 12.5 W m^{-2} C^{-1}. *Seager et al.* [1995] used an atmospheric boundary layer model to estimate this sensitivity to be between 5 W m^{-2} C^{-1} and 15 W m^{-2} C^{-1}.

[7] Subgridscale processes are parameterized by a vertical diffusion and viscosity of 10^{-4} m^2 s^{-1}. Convective overturning is parameterized by increasing the vertical viscosity to 1000 m^2 s^{-1} for statically unstable profiles. Horizontal viscosity and diffusivity are biharmonic with coefficients 10^{12} m^4 s^{-1} and 10^{10} m^4 s^{-1}, respectively. There is also a quadratic bottom drag with coefficient 10^{-3}. The lateral boundary conditions are no-slip for momentum and insulating for temperature. The equation of state is linear in temperature only, so that $\rho = \rho_0 - \alpha(T - T_0)$, where $\rho_0 = 1026$ Kg m^{-3} is a reference density, $T_0 = 12$°C is a reference temperature, and $\alpha = 0.2$ Kg m^{-3} C^{-1} is the thermal expansion coefficient.

[8] The model is initialized at rest with a uniform temperature of 12°C. There is an initial 200 year spin-up period during which the temperature is stepped forward in time with a time step five times larger than that for momentum. The model is then run for another 200 years with synchronis time stepping. The analysis in this paper will be on the final 200 years integration.

[9] The time averaged horizontal transport streamfunction over the final 200 years is shown in Figure 1a. The depth averaged circulation is dominated by the wind-driven gyres, with maximum transports of $O(45 \times 10^6$ m^3 s$^{-1})$. The western boundary current does not penetrate very far into the basin as a steady, coherent feature. This is because of strong synoptic meandering shortly after the boundary current separates from the western boundary.

[10] The mean temperature at 12.5 m depth is shown in Figure 1b. The meridional gradient in temperature is concentrated near the boundary between the subtropical and subpolar gyres. The sharpest gradient is maintained only very close to the western boundary, similar to the transport streamfunction. The broader region of SST gradients through the middle of the domain is a result of strong meandering of SST fronts. The mean mixed layer depth is given by the white contours (depth at which the temperature is 0.2°C colder than at the surface). The region of deepest mixing is confined to the western interior of the subpolar gyre. It is noteworthy that the mixed layer depth along the eastern and northern boundaries is only $O(500$ m) due to lateral advection by the boundary currents. Low resolution models, as are typically used for climate studies, do not sufficiently resolve the narrow wind-driven boundary currents and thus result in too deep mixing along the boundary [*Spall and Pickart*, 2001]. As will be shown in Section 3, the balances along the boundary are key to the mean and variability of the overturning circulation.

[11] The maximum mean meridional overturning streamfunction is of $O(6 \times 10^6$ m^3 s$^{-1})$ (Figure 1c). This is somewhat weaker than is typically found in global-scale thermohaline circulation models, and in the real ocean. This is because the meridional extent of the model domain is fairly small, and the downwelling is balanced by the diffusively-driven upwelling at low- and mid-latitudes. The leading empirical orthogonal function of the meridional overturning streamfunction, which explains 73% of the variance, is shown in Figure 1d (nondimensional, magnitude of the variability is shown later in Figure 3). The variability extends to the bottom and spans the meridional extent of the subpolar gyre, but does not extend into the subtropical gyre.

[12] The temporal variability of the horizontal transport streamfunction is best described by the leading mode of the

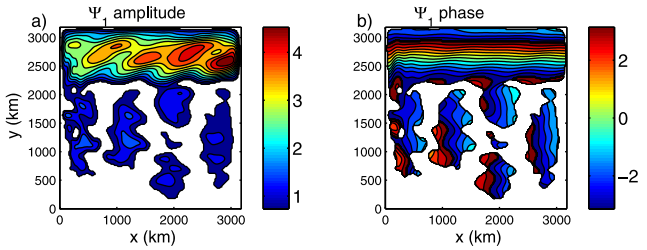

Figure 2. Leading mode of the complex EOF for the horizontal streamfunction: (a) spatial amplitude (Sv) and (b) spatial phase (areas with less than 15% of the maximum spatial amplitude are white).

complex empirical orthogonal function (CEOF, Figures 2a and 2b). This mode accounts for 24% of the total variance of the annual mean streamfunction over the 200 year period, and it explains 41% of the variance in the subpolar gyre. The amplitude is larger in the eastern basin, although the signal extends all the way to the western boundary. Analysis of the streamfunction field indicates that this variability is characterized by alternating zonal jets of meridional scale O(500 km). The phase of the CEOF indicates meridional propagation in time, with nearly uniform phase in longitude. The jets originate near y = 2200 km and propagate northwards. The propagation speed is approximately 0.5 cm s^{-1}, close to the depth averaged meridional velocity forced by the imposed wind stress curl of $v = 2\pi\tau_0/(\rho_0 L\beta H) \approx$ 0.5 cm s^{-1}. This is quite different from the zonal propagation consistent with Rossby waves found by *Huck et al.* [2001], and suggests advection by the mean wind-driven gyre is important. A time series of the amplitude of the CEOF shows variability on time scales of interannual to several decades, with a spectral peak around 7 years. The variability of the MOC shows a similar spectral peak in the 5–10 year band. The dynamical link between the horizontal circulation and the overturning circulation will be demonstrated in the following section.

3. Dynamics of the MOC Variability

[13] The low frequency variability of the horizontal streamfunction is dominated by alternating zonal jets that propagate northwards in the subpolar gyre, similar to those recently observed by *Maximenko et al.* [2005]. While their origins in the real ocean are still not clear, energy conversions in this model run indicate that the variability within the subpolar gyre grows primarily from baroclinic instability of the weak meridional flow due to zonal perturbations acting on the zonal density gradient. The lateral eddy heat flux terms are concentrated in the eastern basin, where the vertical shear in the meridional velocity is the largest, but the perturbations are able to penetrate westward all the way to the western boundary. This is similar to the radiation from unstable meridional eastern boundary currents recently discussed by *Hristova et al.* [2008].

[14] The downwelling component of the MOC is closely tied to active mixing near boundaries. Within the mixed layer, heat loss and vertical mixing force fluid parcels to cross density surfaces yet, away from lateral boundaries, the net mean flow remains horizontal and, to leading order, in geostrophic balance [*Spall and Pickart*, 2001; *Spall*, 2008]. For a cyclonic circulation with downstream decreasing buoyancy, the thermal wind shear forces flow towards the boundary in the upper mixed layer and away from the boundary in the lower mixed layer. This mass budget is closed in the vertical through a narrow viscous boundary layer in which all of the downwelling associated with the net buoyancy loss in the interior takes place [*Spall*, 2008].

[15] These previous studies were derived and analyzed in the context of the mean MOC yet can also be expected to hold for slowly varying flows. The average mixed layer depth and barotropic zonal velocity within 120 km of the northern boundary are shown in Figure 3a as a function of time. The annual average mixed layer depth varies by O(300) m on time scales of 5–10 years. Note that the mean mixed layer depth within the boundary current is 490 m, much less than the mixed layer depth only a short distance away in the interior, which often goes to the bottom (Figure 1). This shallower mixing near the boundary is due to lateral heat advection by the boundary current. The strength of the lateral advection (red line) varies nearly out of phase with the depth of mixing. Strong horizontal advection is followed by a shallowing of the mixed layer. These velocity fluctuations are caused by the arrival of the zonal jets that were described in the previous section. The barotropic velocity is negatively correlated with the mixed layer depth with a magnitude of −0.63 when the velocity leads the mixed layer by 1 year (the 95% confidence level is 0.17), indicating that changes in the velocity drive the changes in the mixed layer depth. When the mixed layer leads the velocity by 1 year, the correlation is weakly positive (0.31). The mixed layer depth at the eastern end of the northern boundary is both shallower and much more constant in time, which shows that the variations in mixed layer depth do not originate upstream in the boundary current.

[16] The previous theories of *Spall and Pickart* [2001] and *Spall* [2008] assert that the MOC is related directly to the mixed layer depth along the boundary with essentially no time lag. This is also supported by the correlation between the annual mean MOC strength and the mixed layer depth, which has maximum value of 0.57 with zero lag. The barotropic velocity is negatively correlated with the MOC with a magnitude of −0.66 when the velocity leads the MOC by 1 year.

[17] *Spall* [2008] assumes that the MOC is controlled by the geostrophic flow towards the boundary, and that this is in turn determined by a balance between along-boundary advection of heat by the boundary current and heat loss to the atmosphere, to derive a prediction of the strength of the MOC, M, as

$$M = \frac{x}{4f_0}\left(\frac{B^3 x}{2N^2U^3}\right)^{1/2} + \frac{h_0 B}{4f_0 U}. \quad (1)$$

The surface buoyancy loss is B, x is the along-boundary distance, N^2 is the Brunt Väisälä frequency in the boundary current below the mixed layer, U is the velocity at the base of the mixed layer, approximated here by the barotropic velocity, and f_0 is the Coriolis parameter (constant). This is a slight modification of the expression derived by *Spall* [2008], where the second term has been added because the

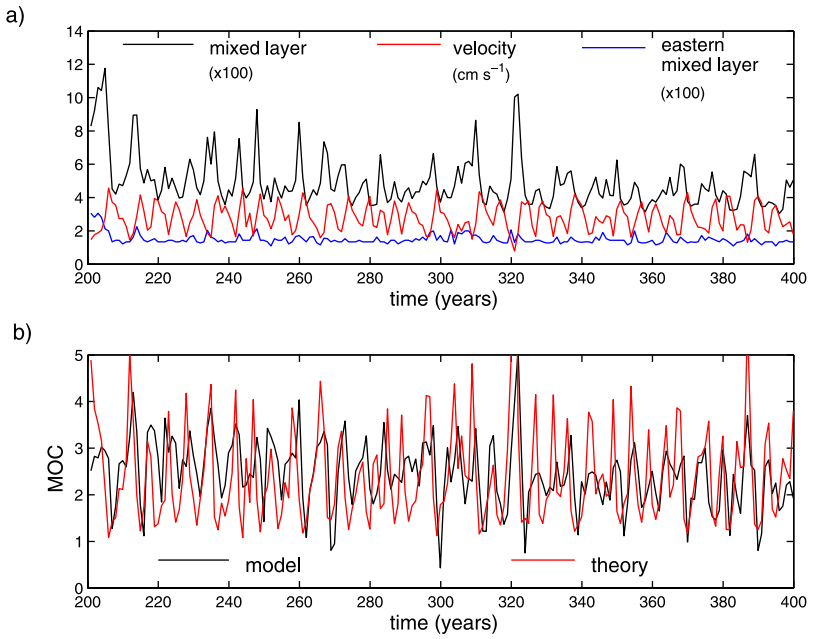

Figure 3. (a) Time series of zonally averaged mixed layer depth (black, 100 s of meters), barotropic velocity (red, cm s^{-1}), and mixed layer depth at 3100 km longitude (blue, 100 s of meters) within 120 km of the northern boundary. (b) Time series of maximum buoyancy-forced meridional overturning circulation (10^6 m^3 s^{-1}) at y = 2400 km (black) and theoretical prediction from (1) using the diagnosed barotropic velocity (red line in Figure 3a) as input (red).

mixed layer depth at $x = 0$ (eastern boundary) is h_0, where it was previously assumed to be zero.

[18] A time series of the annual mean buoyancy-forced MOC diagnosed from the model at y = 2400 km is compared to the MOC predicted by (1) in Figure 3b. The full MOC diagnosed in the model is a combination of the wind-driven MOC and the buoyancy-driven MOC. The model is forced with a wind-stress that is westward at the northern boundary with strength τ_0. This forces an Ekman transport into the northern boundary that will downwell within a narrow boundary layer and return to the interior over the depth of the mixed layer [*Pedlosky*, 1968]. Note that this wind-forced component of the MOC penetrates as deeply as does the buoyancy-forced MOC. This wind-forced MOC is $M_{wind} = \tau_0 L/\rho_0 f_0 = 3.3$ Sv, and is a significant component of the total MOC. Equation (1) predicts only the buoyancy-driven component of the MOC so the (steady) wind-driven component has been subtracted from the full MOC diagnosed from the model. The value of U in (1) is taken from Figure 3a and the stratification is taken as the mean stratification at the eastern end of the northern boundary current at 500 m depth, $N^2 = 1.5 \times 10^{-5}$ s^{-2}. The total net downwelling is calculated using $x = L = 3200$ km and $f_0 = 1.32 \times 10^{-4}$ s^{-1}. For simplicity, the surface buoyancy flux is taken as constant, based on the difference between the mean SST and T_a of 4°C, resulting in $B = 2.2 \times 10^{-8}$ m^2 s^{-3}. The surface heat flux is in phase with the horizontal velocity (weaker boundary current, lower temperature, reduced heat loss) but the resulting heat loss varies by less than 10% of the mean, so, for simplicity, it is taken to be constant here. The prediction agrees reasonably well with the modeled MOC, particularly in terms of the phase of the oscillations. The correlation between the theory and the model MOC has a maximum value of 0.61 when the theory leads by 1 year, consistent with the delay previously discussed due to restratification. Most of the variability in the MOC results from the first term, which represents the change in mixed layer depth along the boundary that results from changes in the lateral advection speed. The second term contributes approximately 0.75 Sv to the mean MOC and is relatively constant in time. The general agreement between the theory and model MOC indicates that both the mean and variability of the MOC are determined by the depth of the mixed layer and change in density within the mixed layer along the northern boundary. The mixed layer, in turn, is controlled by a balance of lateral advection and surface cooling. For stratification and cooling rates that are constant in time, time dependence of the MOC is due entirely to time dependence in the strength of the boundary current U.

[19] The strength of the internal variability in the model is sensitive to the restoring time scale used to produce the surface heat flux. If the relaxation time scale is decreased to 30 days, or increased to 200 days, the internal variability of the horizontal transport streamfunction and the overturning streamfunction are both reduced significantly. For the case of strong relaxation, thermal anomalies are damped quickly, while for the case of weak relaxation, the baroclinic shear in the eastern basin and the zonal jets produced by baroclinic instability are both weaker. Although this particular mode of internal variability is sensitive to the model parameters, the more important point is that the basic relationship between the horizontal and overturning gyres, as described by (1), still holds for these cases. The mean MOC in a calculation without wind-forcing is stronger and penetrates much deeper along the northern boundary. The zonal perturba-

tions are not produced, supporting the interpretation that they are due to baroclinic instability of the wind-forced circulation, and the low frequency variability of the MOC is much weaker, consistent with the zonal jets being the driver of the MOC variability in the wind-forced cases.

4. Conclusions

[20] A high resolution, idealized model of the wind- and buoyancy-driven oceanic general circulation is used to demonstrate a close connection between the horizontal and overturning gyres. In this particular case, the low frequency variability of the horizontal circulation is dominated by alternating zonal jets within the subpolar gyre. These jets enhance or reduce the transport in the cyclonic boundary current that encircles the northern boundary, and directly influence the depth of mixing along the boundary. A simple theory that assumes that the overturning circulation is determined by the pressure gradient along the boundary reproduces well the mean and low frequency variability of the overturning circulation diagnosed from the model. The variability in the MOC is driven by variability in the barotropic transport near the northern boundary.

[21] The wind-forced circulation modifies the deep mixing in two important ways. First, it advects heat northwards in the eastern basin, maintaining a zonal temperature gradient over much of the interior. In fact, the gyre heat transport dominates the overturning heat transport in the subpolar gyre in this calculation. It is this zonal temperature gradient that provides the source for the instabilities that produce the zonal jets. The second important role of the wind-forced circulation is to advect heat along the northern boundary, thus inhibiting deep mixing there. This plays a leading order role in shaping the magnitude and depth of the meridional overturning circulation through the dynamics of sinking motions [*Spall*, 2008]. These dynamics are also likely to be important for externally forced variability, such as might arise from variability in the wind stress, ice cover, or freshwater runoff.

[22] **Acknowledgments.** This work was supported by NSF grants OCE-0423975 and OCE-0726339.

References

Dijkstra, H. A., and C. A. Katsman (1997), Temporal variability of the wind-driven quasi-geostrophic double gyre ocean circulation: Basic bifurcation diagrams, *Geophys. Astrophys. Fluid Dyn.*, *85*, 195–232.

Hristova, H. G., J. Pedlosky, and M. A. Spall (2008), Radiating instability of a meridional boundary current, *J. Phys. Oceanogr.*, in press.

Huck, T., G. K. Vallis, and A. Colin de Verdiere (2001), On the robustness of the interdecadal modes of the thermohaline circulation, *J. Clim.*, *14*, 940–963.

Marshall, J., C. Hill, L. Perelman, and A. Adcroft (1997), Hydrostatic, quasi-hydrostatic, and nonhydrostatic ocean modeling, *J. Geophys. Res.*, *102*, 5733–5752.

Maximenko, N., B. Bang, and H. Sasaki (2005), Observational evidence of alternating zonal jets in the world ocean, *Geophys. Res. Lett.*, *32*, L12607, doi:10.1029/2005GL022728.

Pedlosky, J. (1968), An overlooked aspect of the wind-driven oceanic circulation, *J. Fluid Mech.*, *32*, 809–821.

Seager, R., Y. Kushnir, and M. A. Cane (1995), On heat flux boundary conditions for ocean models, *J. Phys. Oceanogr.*, *25*, 3219–3230.

Spall, M. A. (1994), Mechanism for low-frequency variability and salt flux in the Mediterranean salt tongue, *J. Geophys. Res.*, *99*, 10,121–10,129.

Spall, M. A. (2008), Buoyancy-forced downwelling in boundary currents, *J. Phys. Oceanogr.*, in press.

Spall, M. A., and R. S. Pickart (2001), Where does dense water sink? A subpolar gyre example, *J. Phys. Oceanogr.*, *31*, 810–826.

M. A. Spall, Physical Oceanography Department, Woods Hole Oceanographic Institution, Woods Hole, MA 02543, USA. (mspall@whoi.edu)